

Supporting Information for:
Remote Non-Genetic Optical Modulation of Neuronal Activity using Fuzzy Graphene

Sahil K. Rastogi^{a,1}, Raghav Garg^{b,1}, Matteo Giuseppe Scopelliti^c, Bernardo I. Pinto^d, Jane E. Hartung^e, Seokhyoung Kim^f, Corban G.E. Murphey^f, Nicholas Johnson^b, Daniel San Roman^b, Francisco Bezanilla^d, James F. Cahoon^f, Michael S. Gold^e, Maysam Chamanzar^c, Tzahi Cohen-Karni^{a,b,*}

a Department of Biomedical Engineering, Carnegie Mellon University, Pittsburgh, PA, 15213, USA.

b Department of Materials Science and Engineering, Carnegie Mellon University, Pittsburgh, PA, 15213, USA.

c Department of Electrical and Computer Engineering, Carnegie Mellon University, Pittsburgh, PA, 15213, USA.

d Department of Biochemistry and Molecular Biology, University of Chicago, Chicago, IL, 60637, USA.

e Department of Neurobiology, University of Pittsburgh, Pittsburgh, PA, 15213, USA.

f Department of Chemistry, University of North Carolina at Chapel Hill, Chapel Hill, NC, 27599-3290, USA.

1 These authors contributed equally to this work.

* **Corresponding author:** Tzahi Cohen-Karni

Email: tzahi@andrew.cmu.edu

This PDF file includes:

Supplementary materials and methods

Additional notes

Figures S1 to S22

Legends for Movies S1 and S2

Tables S1 to S13

References

Other supplementary materials for this manuscript include the following:

Movies S1 and S2

Supplementary materials and methods

Raman spectroscopy. Raman spectroscopy was performed using NT-MDT NTEGRA Spectra with 532 nm and 633 nm excitations through a 100× objective for single and dual laser Raman analysis (1, 2). Briefly, 10 µL NT-3DFG suspension was drop casted onto a bond pad array and bright field optical images were acquired. Raman spectra from individual NT-3DFGs were then acquired with 0.5 ND filter and an acquisition time of 30 s. Raman spectra from the same point on individual wires were acquired using dual lasers- 532 nm and 633 nm, and G dispersion ($Disp(G)$) values were computed using:

$$Disp(G) = \left| \frac{Pos(G)_{633nm} - Pos(G)_{532nm}}{\lambda_{633nm} - \lambda_{532nm}} \right|$$

$Pos(G)$, and λ are the position of the G peak with a specific excitation laser and the excitation laser wavelength, respectively (3). Raman spectra was acquired from 90 wires across 3 independent samples.

X-ray photoelectron spectroscopy (XPS). XPS was conducted using an Escalab 250Xi (Thermo Scientific) with Al K α (1486.68 eV) X-ray source at ultra-high vacuum (10^{-9} Torr). Survey spectra were acquired by averaging 5 scans with a 120 eV pass energy, 15 ms acquisition time, and 0.5 eV step size. C1s, O1s and N1s spectra were acquired by averaging 10 scans with a 50 eV pass energy, 50 ms acquisition time, and 0.1 eV step size. Compositional and chemical state analyses were performed using Thermo Scientific Advantage peak fitting software.

UV-Vis spectroscopy. i-SiNW and NT-3DFG meshes were synthesized on 1.5 cm × 1.5 cm fused silica (University Wafer, catalog no. 1013) substrates following a previously published protocol (1). Briefly, i-SiNWs were synthesized on fused silica substrates using AuNP catalyzed VLS growth process as explained above. The synthesized NWs were collapsed to form a mesh by flowing liquid N₂ into the CVD quartz tube under 200 sccm Ar flow, followed by a 10 min annealing step at 800°C under 200 sccm H₂ flow at 1.6 Torr. For NT-3DFG meshes, the annealed i-SiNW samples were introduced in the PECVD system followed by 3DFG synthesis for 5, 10, 30, and 90 min. UV-Vis spectra were acquired using OL 770 multi-channel spectroradiometer (Optronic Laboratories, Inc.) with Xenon light source and integrating sphere. The transmittance and reflectance for each sample type were measured with bare fused silica as a reference. The absorbance was calculated as:

$$Absorbance = 1 - (Reflectance + Transmittance)$$

Measurements were performed on n = 3 per sample type, and mean spectra were plotted.

Spheroid immunostaining. NT-3DFG interfaced cortical spheroids were transferred to a sterile polystyrene petri dish (VWR). The culture media was serially exchanged with 1× PBS. The spheroids were then fixed using 4% paraformaldehyde (Electron Microscopy Sciences, catalog no. 15710) in 1× PBS for 20 min on a shaker at room temperature. The fixed spheroids were then gently rinsed 3 times with 1× PBS for 5 min each time on a shaker at room temperature. 1× PBS was replaced with blocking solution composed of 5% goat serum (ThermoFisher, catalog no. 16210-064) and 0.4% Triton-X (Sigma-Aldrich, catalog no. X-100) in 1× PBS and the samples were incubated on a shaker for 2 h at room temperature. The samples were gently rinsed 3 times with 1× PBS for 5 min each time on a shaker at room temperature. The samples were then incubated with primary antibody solution composed of 0.5% β -tubulin III rabbit mAb (Cell Signaling Technologies, catalog no. 5568S), 5% goat serum and 0.1% Triton-X in 1× PBS on a shaker for 48 h at 4 °C. Primary antibody solution was rinsed 3 times with 1× PBS for 5 min each time on a shaker at room temperature. The samples were then incubated with secondary antibody solution composed of 0.2% anti-rabbit IgG Alexa Fluor 647 (Cell Signaling Technologies, catalog no. 4414S), 0.2% anti-mouse IgG Alexa Fluor 555 (Cell Signaling Technologies, catalog no. 4409S), 0.2 µg/mL DAPI (ThermoFisher, catalog no. 62248), and 5% goat serum in 1× PBS on a shaker for 24 h at room temperature. The samples were rinsed 3 times with 1× PBS for 5 min each time on a shaker at room temperature and imaged using upright confocal microscope and a 20×/0.50 NA water immersion objective. Minimum intensity DIC projection, maximum intensity 3D reconstruction, and z-sections were generated using NIS elements (Nikon).

Dispersing NT-3DFG throughout cortical spheroid. In order to disperse NT-3DFG throughout the bulk of cortical spheroids, 2 μL /mold of NT-3DFG suspension was mixed with 188 μL /mold of cell suspension (500,000 cells per mold). The prepared cell suspension was then seeded into agarose molds. The spheroids were imaged after 7 days in vitro.

Additional notes

Raman spectroscopy of NT-3DFG. The presence of characteristic peaks in the Raman spectra, i.e., D, G, and 2D peaks, confirms the presence of graphene (Fig. S3a, Table S1). The emergence of the D peak, at ca. 1335 cm^{-1} , and the D' peak, as a shoulder to the G peak, is attributed to the breaks in translational symmetry due to the presence of 3DFG edges, as evident in the SEM and TEM images (Figs. 1, S1, and S2) (4, 5). The broad symmetric 2D peak can be attributed to the presence of juxtaposed single-to-few layer graphene flakes (6, 7). The appearance of a strong D peak due to edge effects was further verified by dual-wavelength Raman spectroscopy. The lack of clear correlation between I_D/I_G and dispersion of G peak (Disp(G)) as well as between I_D/I_G and full width at half-maximum of G peak (FWHM(G)) (Fig. S3b, c, and Table S2) confirms that the major contribution to the D peak is due to edge defects rather than bulk-structural defects (1, 7). Furthermore, the saturation of Disp(G) at $0.2\text{ cm}^{-1}/\text{nm}$ (Fig. S3b), indicates the presence of sp^2 hybridization and lack of large structural defects (1, 8).

X-ray photoelectron (XPS) spectroscopy of NT-3DFG before and after surface modification. Surface chemistry of the pristine as well as surface-modified NT-3DFGs was investigated using XPS characterization (Fig. S4). XPS was performed on pristine NT-3DFG (Fig. S4a I, b I-III, Table S4), HNO_3 -treated NT-3DFG (Fig. S4a II, c I-III, Table S4), and HNO_3 -treated and KF modified NT-3DFG (Fig. S4a III, d I-III, Table S4). Presence of a prominent sp^2 hybridized C1s peak at ca. 284 eV in all three conditions (Fig. S4b I, c I, d I, Table S5) corroborates the presence of sp^2 C lattice of graphene (9-11). The peak at ca. 290 eV is attributed to $\pi \rightarrow \pi^*$ shake up satellite feature (2). The peaks at 285.7, 286.8 and 288.1 in C1s spectra of HNO_3 -treated NT-3DFG (Fig. S4c I, Table S5), and HNO_3 -treated and KF modified NT-3DFG (Fig. S4d I, Table S5) is due to presence of C-O, C=O and O-C=O and/or N-C=O bonds, respectively (12-14), which is attributed to the formation of oxide groups due to nitric treatment (15) and amide bonds in peptides (16). The peak at ca. 532 and 533 eV in the O1s spectra (Fig. S4b II, c II, d II, Table S5) is due to presence of C=O and C-O bonds, respectively (16, 17). The low intensity of O1s peak in case of pristine sample (Fig. S4a I, Tables S4 and S5) might be attributed to adsorption of organic contaminants (18). The increase in the C-O and C=O peak intensity in the case of HNO_3 -treated and KF modified NT-3DFG samples (Fig. S4a II, III) can be attributed to presence of oxide species due to HNO_3 treatment (15). The further increase in the C=O peak in the KF modified NT-3DFG can be attributed to the presence of C=O groups in the peptide backbone (16). The peak at ca. 406 eV in the N1s spectra of both HNO_3 treated NT-3DFG (Fig. S4c III, Table S5) and KF modified NT-3DFG (Fig. S4d III, Table S5) samples is due to NO_3^- groups which can be attributed to the treatment with HNO_3 (19, 20). The amide peak at ca. 400 eV in the N1s spectra for KF-modified NT-3DFG samples (Fig. S4d III, Table S5) confirms the presence of peptides on the NT-3DFG surface (12, 13, 16).

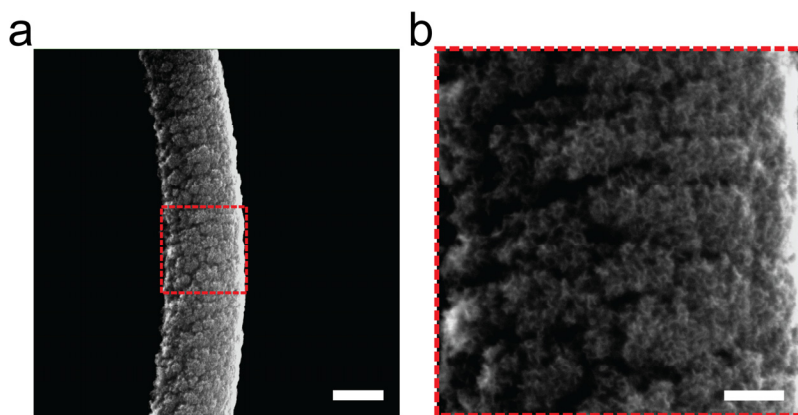
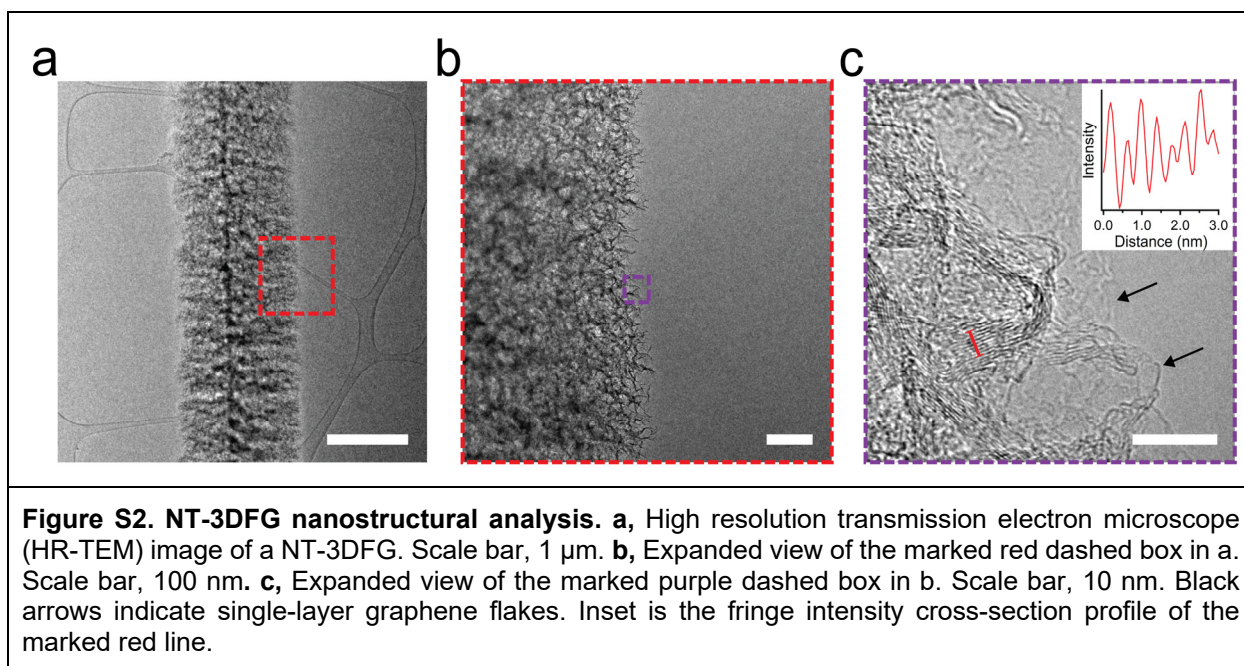


Figure S1. Morphology of dispersed NT-3DFG. **a**, Representative scanning electron microscope (SEM) image of a NT-3DFG drop casted on an indium tin oxide (ITO) substrate. Scale bar, 1 μm . **b**, Expanded view of the marked red dashed box in **a**. Scale bar, 250 nm.



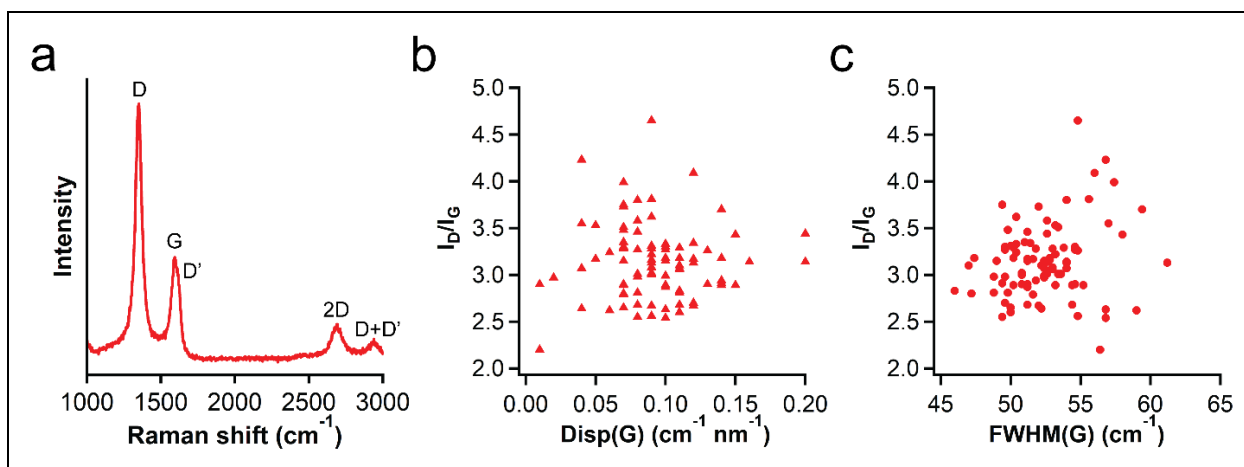


Figure S3. Raman spectroscopy of NT-3DFG. **a**, Representative Raman spectrum of a drop-casted NT-3DFG ($n = 90$ independent NT-3DFGs). **b**, Peak intensity ratio of D peak to G peak (I_D/I_G) as a function of dispersion of G peak. **c**, Peak intensity ratio of D peak to G peak (I_D/I_G) as a function of FWHM of G peak ($n = 90$ independent NT-3DFGs).

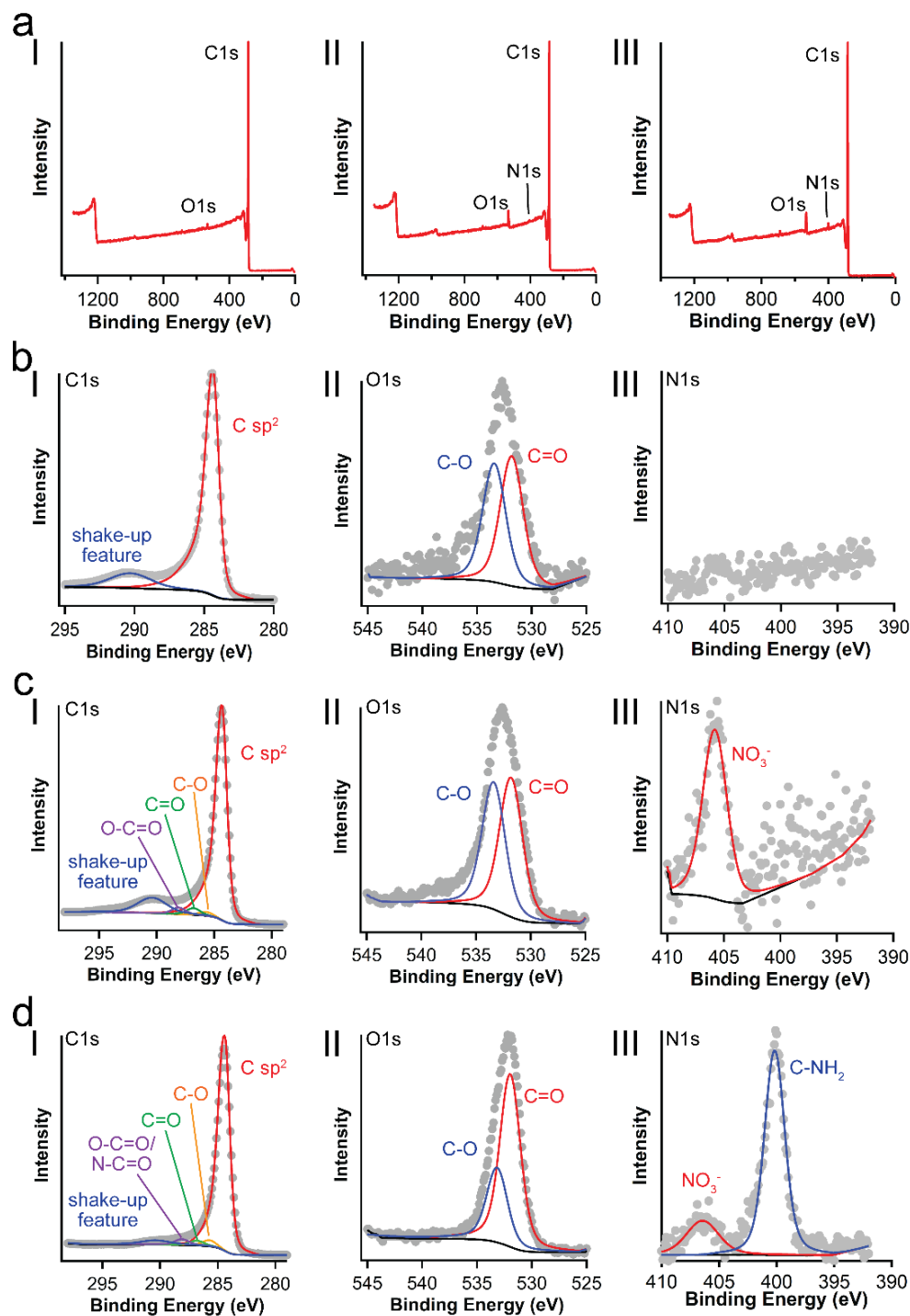


Figure S4. NT-3DFG surface modification analysis. **a**, Representative X-ray photoelectron spectroscopy (XPS) survey of (I) pristine NT-3DFG, (II) HNO₃-treated NT-3DFG, and (III) HNO₃-treated and lysine-phenylalanine based peptide (KF)₄-modified NT-3DFG. **b-d**, Representative (I) C1s, (II) O1s and (III) N1s spectra of **b**, pristine NT-3DFG, **c**, HNO₃-treated NT-3DFG, and **d**, HNO₃-treated and (KF)₄ modified NT-3DFG. Solid grey circles denote raw data. Data was acquired for n = 3 independent samples for each condition.

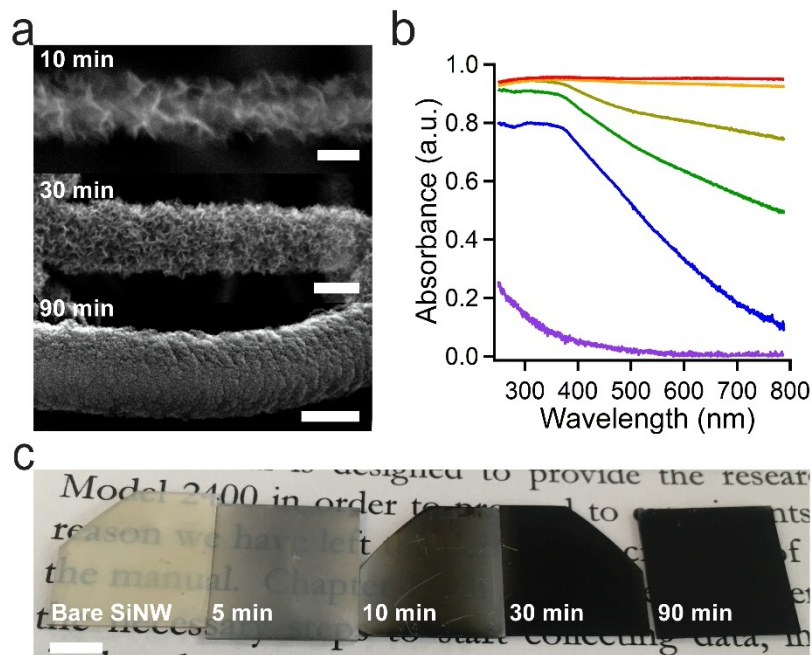


Figure S5. High absorbance of NT-3DFG meshes. **a**, SEM images of NT-3DFG synthesized for 10 min, 30 min and 90 min. Scale bars, 100 nm, 250 nm, and 1 μ m, respectively. **b**, Mean UV-Vis spectra of fused silica (purple), bare i-Si nanowire mesh (blue), and NT-3DFG meshes synthesized for 5 min (green), 10 min (brown), 30 min (orange), and 90 min (red) ($n = 3$). **c**, Optical image of SiNWs and NT-3DFG meshes synthesized for 5 min, 10 min, 30 min and 90 min, on fused silica substrates. Scale bar, 5 mm.

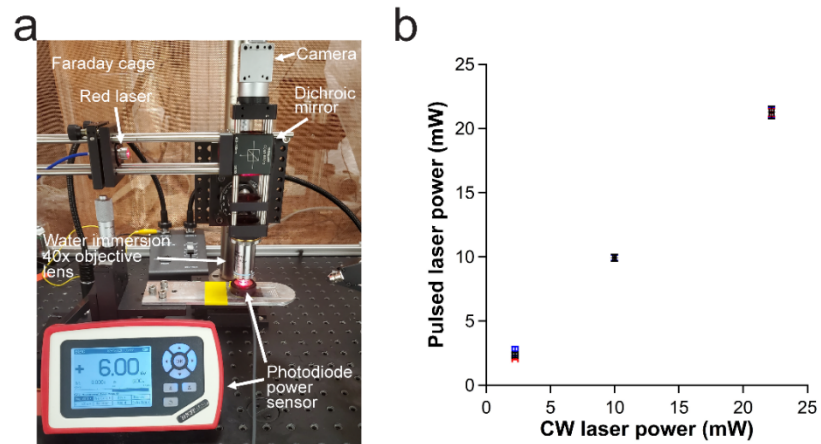


Figure S6. Laser power output characterization. **a**, Custom-built single-photon microscope with photodiode power sensor for characterizing the performance of the laser. **b**, Pulsed laser power as a function of the continuous-wave (CW) laser power for the 635 nm laser with 0.1 (red), 1.0 (blue), and 10.0 (black) pulses. Results are presented as mean \pm SD (10 pulses per pulsing condition).

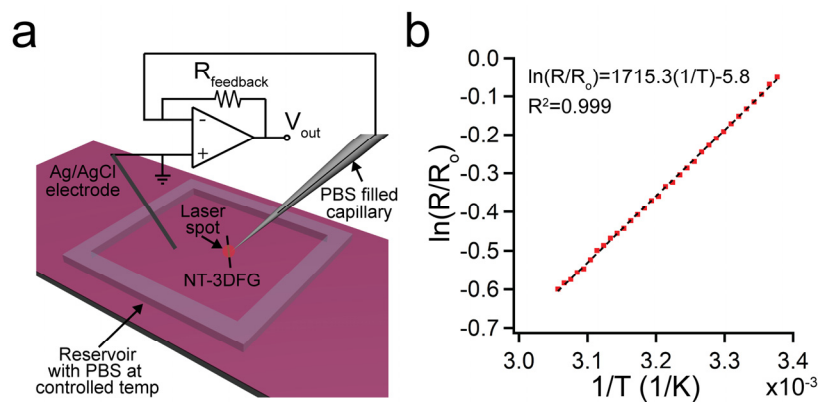


Figure S7. Photothermal characterization of NT-3DFG. **a**, Schematics of the photothermal characterization of a drop casted NT-3DFG. **b**, Resistance versus temperature calibration curve for a pipette with a measured resistance of 1.9 MΩ at room temperature. Black dashed line denotes the linear fit.

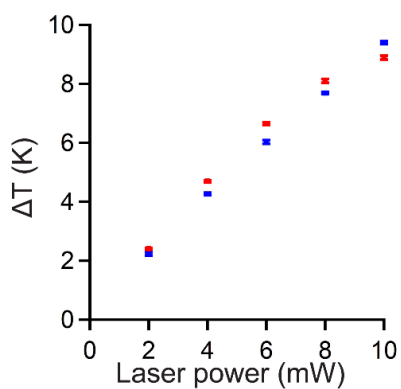


Figure S8. Photothermal effect in NT-3DFG under different wavelengths. Temperature change as a function of power of 405 nm (blue) and 635 nm (red) laser (20 μm spot size, 10 ms pulse) for a representative isolated NT-3DFG. Results are presented as mean \pm SD (n = 10 measurements per wire).

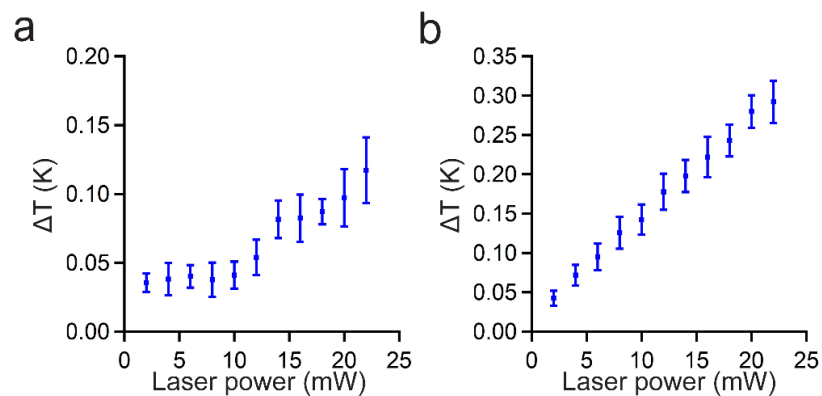


Figure S9. Photothermal effect in bare i-SiNWs. Temperature change as a function of power of the incident laser (635 nm laser, 20 μm spot size) for a representative isolated bare i-SiNW (blue) under **a**, 1 ms and **b**, 10 ms laser pulse widths. Results are presented as mean \pm SD ($n = 10$ measurements per wire).

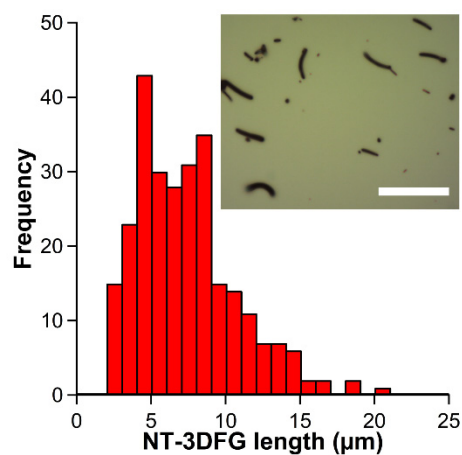


Figure S10. NT-3DFG length distribution. NT-3DFG length distribution for suspension prepared for NT-3DFG concentration viability assay (270 nanowires measured across 4 samples). Inset is a representative optical image of the NT-3DFG suspension as drop-casted on a Si/SiO₂ chip. Scale bar, 20 μm. NT-3DFG suspension prepared via sonication at 20 kHz and 36 W for 1 min using a probe sonicator.

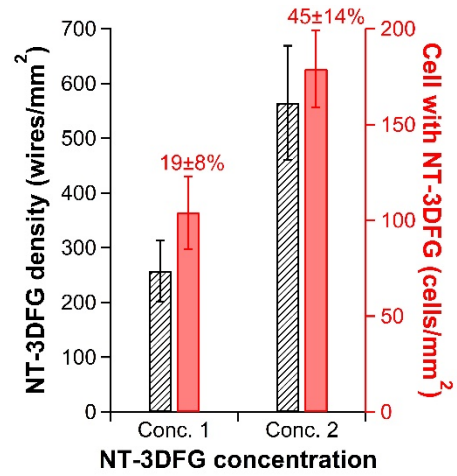
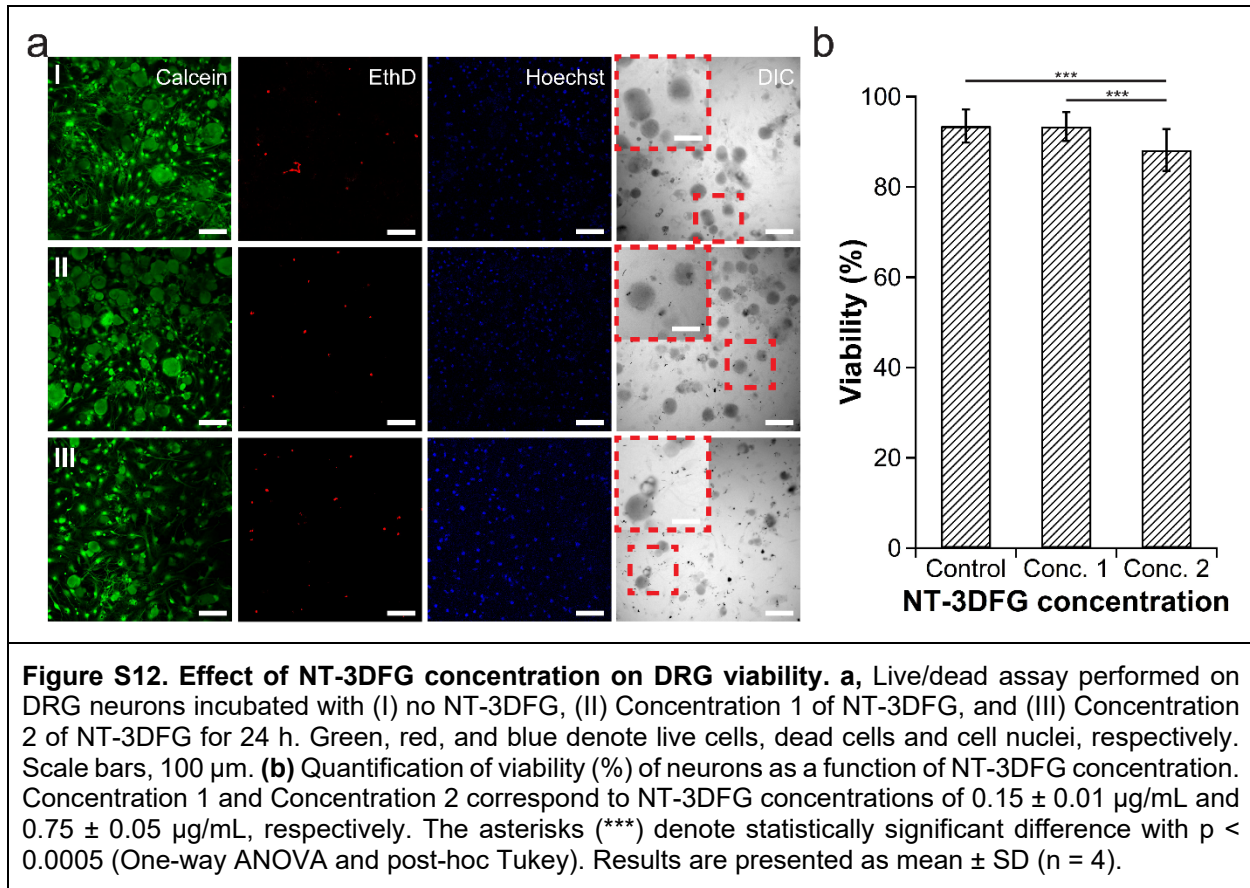


Figure S11. NT-3DFG distribution in DRG cell culture. Areal distribution of NT-3DFG and cells with NT-3DFG as measured for Concentration 1 ($0.15 \pm 0.01 \mu\text{g/mL}$) and Concentration 2 ($0.75 \pm 0.05 \mu\text{g/mL}$). Results are presented as mean \pm SD ($n = 4$, 10 images per independent sample).



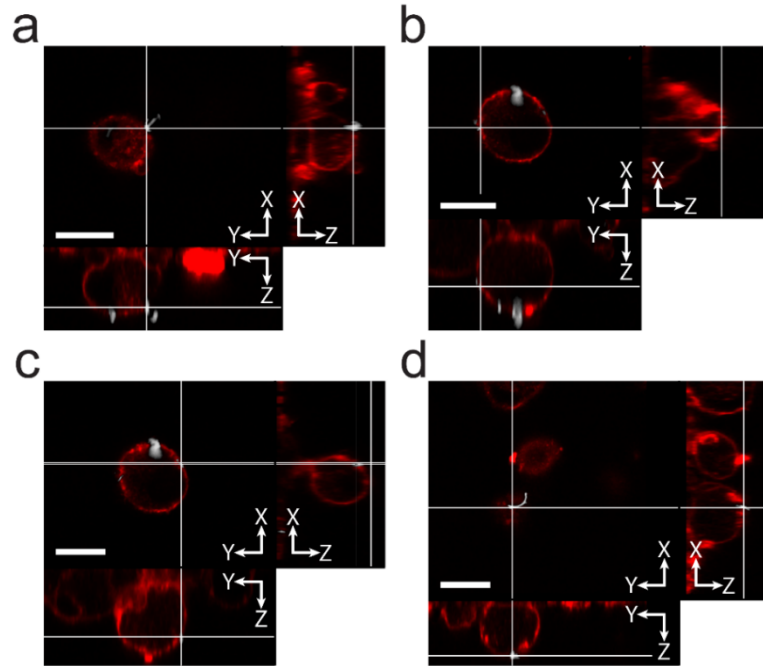


Figure S13. Interface between DRG neurons and NT-3DFG. a-d, Orthogonal sections of fluorescent images of representative DRG neurons labeled with CellMask plasma membrane stain (red) and interfaced with NT-3DFG (white). Scale bars, 20 μm.

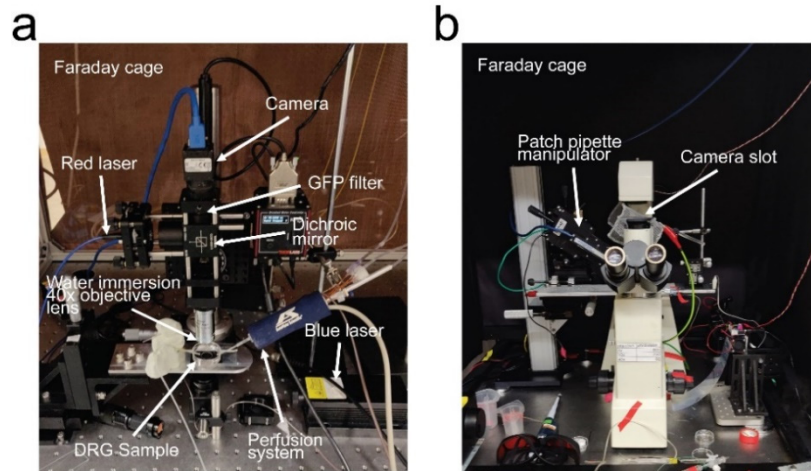


Figure S14. Photothermal stimulation: microscope setups. **a**, Custom-built single-photon microscope for photothermal characterization of NT-3DFG, and calcium imaging of neurons during photothermal stimulation. **b**, Custom-built microscope setup for concurrent patch clamp measurements of neurons and photothermal stimulation.

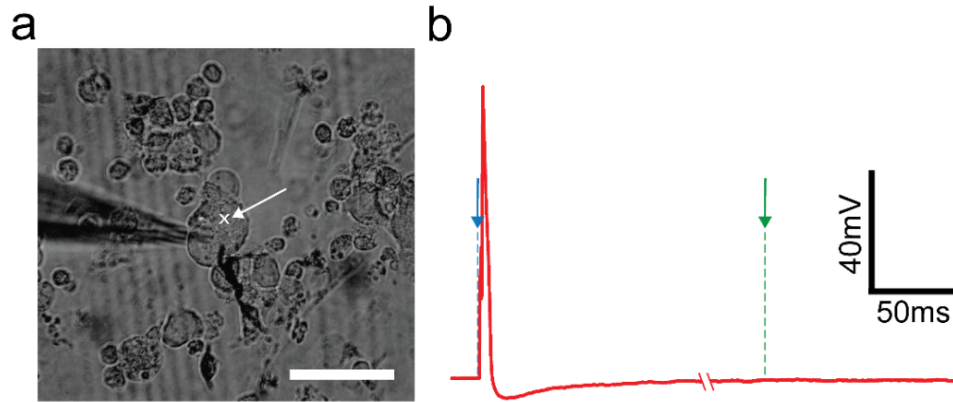


Figure S15. Off-NT-3DFG laser illumination – DRG neuron. **a**, Bright field image of a DRG neuron interfaced with NT-3DFG. White cross indicates the point where the laser pulse was applied. Scale bar, 50 μm . **b**, A representative membrane potential recorded using whole cell patch clamp of a DRG neuron illuminated by a 405 nm laser with 1.2 ms pulse duration and 3.02 mW applied power (3.62 μJ). Blue and green arrows represent the time points when the electrical and the optical stimulation pulses were applied, respectively.

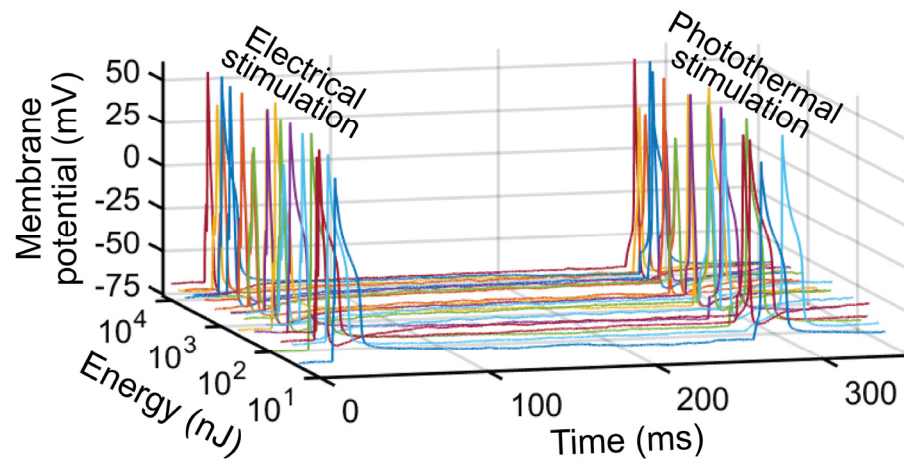


Figure S16. Photothermal stimulation at varying laser energies. Membrane potential recorded using whole cell patch clamp of DRG neurons at varying laser energies ranging from 27 nJ to 10 μ J.

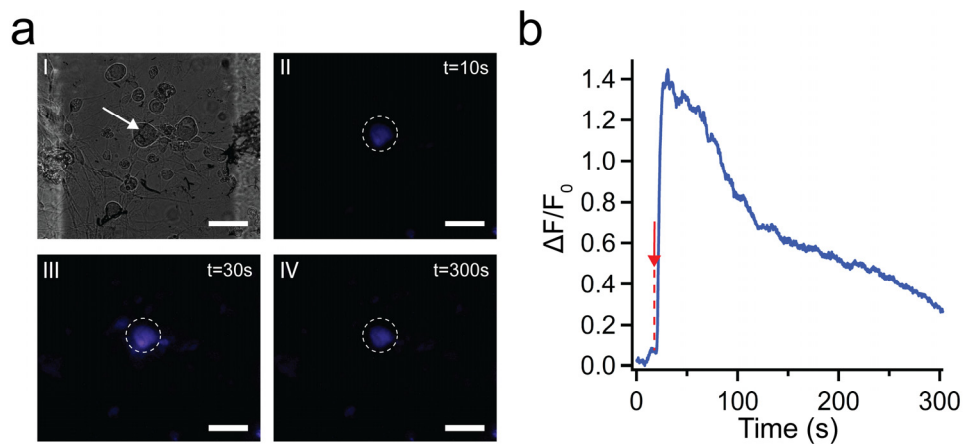
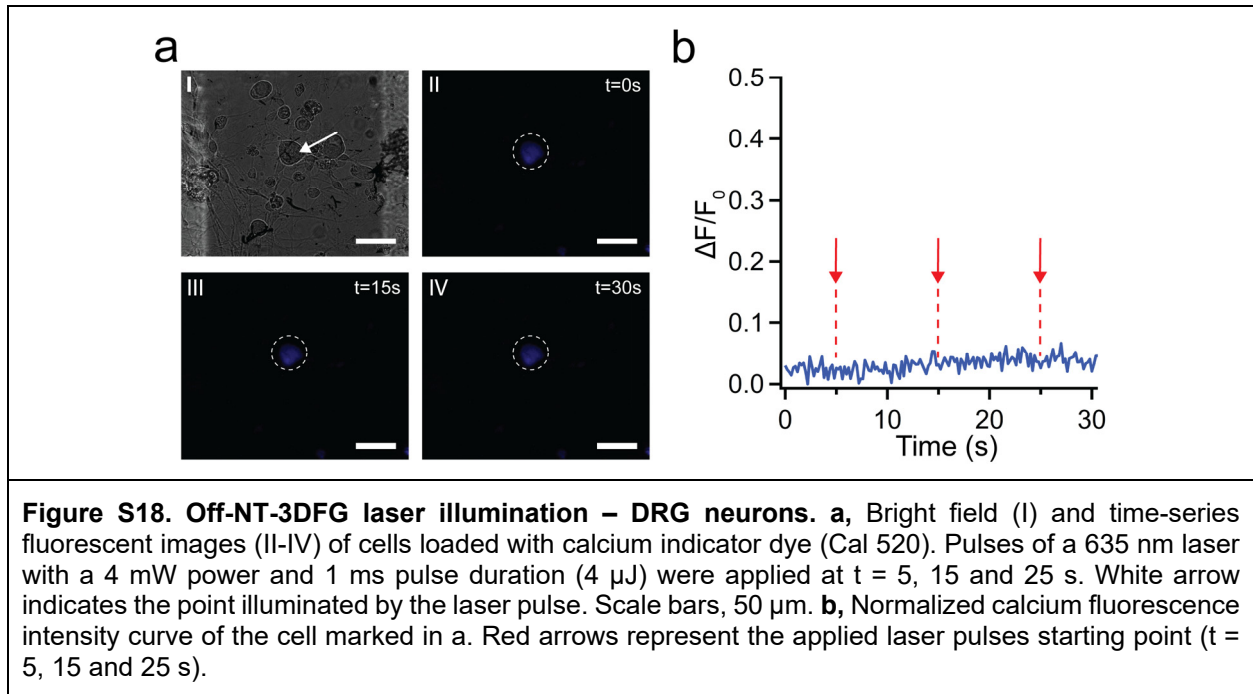


Figure S17. Photothermal stimulation of a DRG neuron. **a**, Bright field (I) and time-series fluorescent images (II-IV) of cells loaded with calcium indicator dye (Cal 520). A pulse of 635 nm laser with 4 mW power and 1 ms pulse duration (4 μ J) was applied at $t = 25$ s. White arrow indicates the NT-3DFG illuminated by the laser pulse. Scale bars, 50 μ m. **b**, Normalized calcium fluorescence intensity curve of the cell marked in a. Red arrow represents the applied laser pulse starting point ($t = 25$ s).



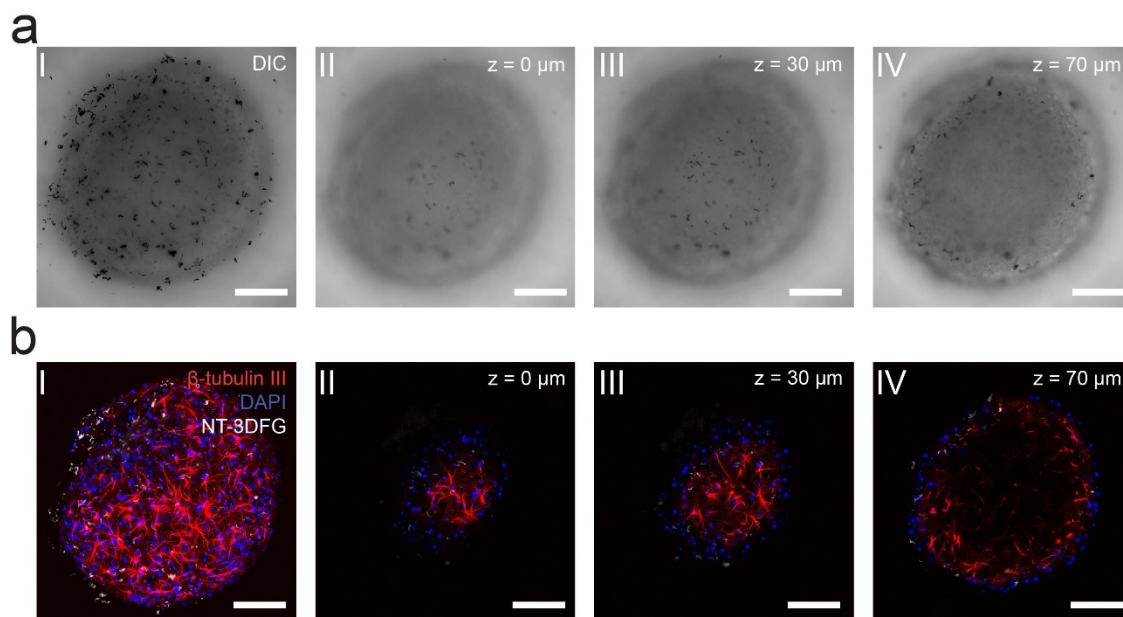
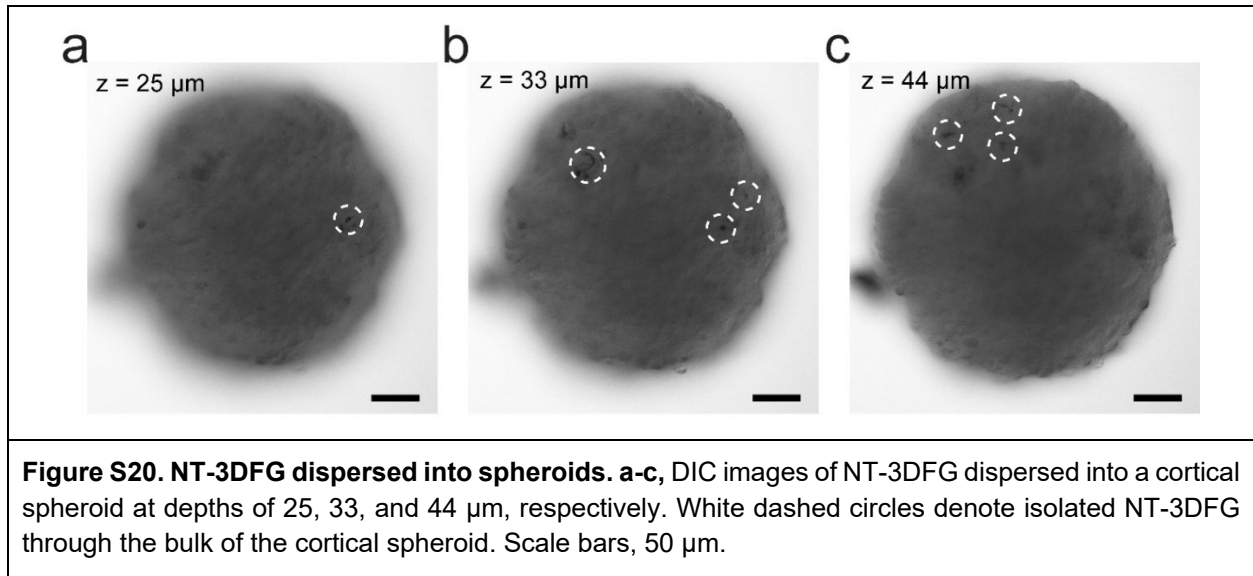


Figure S19. Cortical spheroid and NT-3DFG interfaces. **a**, DIC images of a representative NT-3DFG loaded cortical spheroid presented (I) as a minimum intensity projection, at depths of (II) 0, (III) 30, and (IV) 70 μm . Scale bars, 100 μm . **b**, Fluorescent images of a representative NT-3DFG (white) loaded cortical spheroid immuno-stained with β -tubulin III (red) and DAPI (blue) presented (I) as a maximum intensity 3D reconstruction, at depths of (II) 0, (III) 30, and (IV) 70 μm . Scale bars, 100 μm .



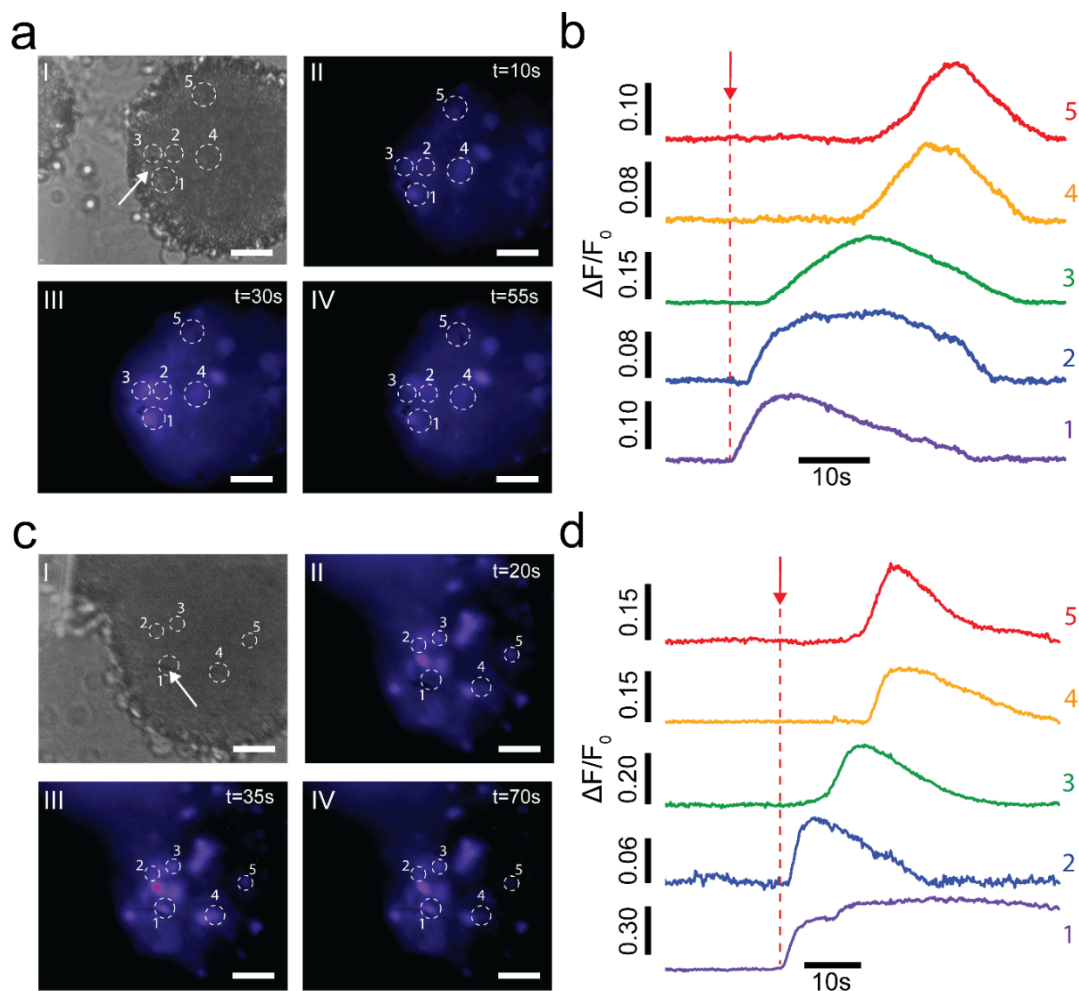


Figure S21. Photothermal stimulation of 3D cortical spheroids. **a, c,** Representative bright field (I) and time-series fluorescent images (II-IV) of cortical spheroids loaded with calcium indicator dye (Cal 520). A 635 nm laser with pulse of 6 mW power and 1 ms pulse duration (6 μJ) was applied at $t = 10$ s (a) and 20 s (c). White arrows represent the NT-3DFG illuminated by the laser pulse. Scale bars, 40 μm . **b, d,** Normalized calcium fluorescence intensity curves of the cells marked in a and c, respectively. Red arrow represents the applied laser pulse starting point.

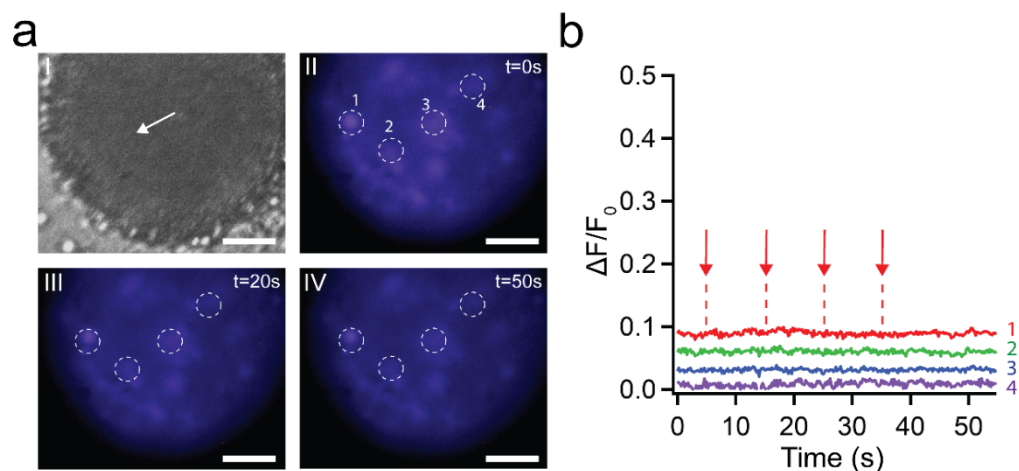


Figure S22. Off-NT-3DFG illumination – 3D cortical spheroid. **a**, Bright field (I) and time-series fluorescent images (II-IV) of cells loaded with calcium indicator dye (Cal 520). Pulses of a 635 nm laser with 6 mW power and 1 ms pulse duration (6 μ J) were applied at $t = 5, 15, 25$ and 35 s. White arrow indicates the point illuminated by the laser pulse. Scale bars, 50 μ m. **b**, Normalized fluorescence intensity curve of the cell marked in **a**. Red arrows represent the applied laser pulses starting point ($t = 5, 15, 25$ and 35 s). The curves were offset along y-axis for ease of presentation.

Movie S1. Photothermal stimulation of a 2D DRG network. Calcium imaging of a DRG network loaded with calcium indicator dye (Cal 520). A 635 nm laser with pulse of 4 mW power and 1 ms pulse duration was applied at $t = 5$ s. Video was acquired at 5 frames per sec, processed in ImageJ, and compressed to mp4 format and sped up by 10 \times .

Movie S2. Photothermal stimulation of a 3D cortical spheroid. Calcium imaging of a cortical spheroid loaded with calcium indicator dye (Cal 520). A 635 nm laser with pulse of 6 mW power and 1 ms pulse duration was applied at $t = 25$ s. Video was acquired at 5 frames per sec, processed in ImageJ, and compressed to mp4 format and sped up by 10 \times .

Table S1. Data summary of Raman analysis of isolated NT-3DFG.

Sample	I_D/I_G	I_{2D}/I_G	Position(D) (cm^{-1})	Position(G) (cm^{-1})	Position(2D) (cm^{-1})	FWHM(G) (cm^{-1})	FWHM(2D) (cm^{-1})
90 min NT-3DFG	3.14 ± 0.40	0.50 ± 0.05	1347.0 ± 3.0	1585.6 ± 4.6	2685.2 ± 6.2	52.4 ± 5.0	93.0 ± 11.2

Table S2. Data summary of dual laser Raman analysis of isolated NT-3DFG.

Sample	NT-3DFG	I_D/I_G	FWHM(G) (cm^{-1})	Disp(G) ($\text{cm}^{-1} \text{ nm}^{-1}$)
N=1	1	3.43	58.0	0.15
	2	3.06	53.0	0.11
	3	3.58	52.6	0.08
	4	2.87	51.2	0.10
	5	3.14	54.0	0.16
	6	2.67	52.0	0.09
	7	3.34	51.4	0.12
	8	3.33	50.4	0.10
	9	2.89	55.2	0.14
	10	3.10	52.2	0.11
	11	2.65	50.0	0.07
	12	3.17	51.2	0.05
	13	3.80	54.0	0.08
	14	2.91	49.4	0.14
	15	3.15	49.0	0.10
	16	2.54	56.8	0.10
	17	3.27	54.6	0.10
	18	2.67	52.0	0.12
	19	2.56	54.8	0.09
	20	3.13	61.2	0.09
	21	3.28	53.0	0.07
	22	3.07	54.0	0.04
	23	2.81	49.8	0.11
	24	3.16	52.8	0.09
	25	2.89	54.4	0.10
	26	2.98	49.6	0.08
	27	2.80	47.2	0.07
	28	2.98	48.8	0.08
	29	3.73	52.0	0.07
	30	2.55	49.4	0.08
N=2	1	3.30	54.6	0.10
	2	3.18	52.8	0.11
	3	3.10	47.0	0.11
	4	2.20	56.4	0.01
	5	2.90	51.2	0.13
	6	3.28	51.8	0.09

	7	3.14	52.6	0.2
	8	2.70	49.6	0.12
	9	2.97	52.4	0.02
	10	2.63	56.8	0.10
	11	3.15	51.2	0.10
	12	3.15	52.4	0.07
	13	3.29	53.8	0.07
	14	3.01	52.6	0.08
	15	3.02	50.8	0.09
	16	4.23	56.8	0.04
	17	2.99	52.4	0.10
	18	3.22	53.2	0.09
	19	2.64	52.2	0.04
	20	2.79	51.6	0.07
	21	2.89	50.2	0.07
	22	3.53	53.2	0.05
	23	3.01	53.4	0.09
	24	2.81	48.8	0.08
	25	3.13	54.0	0.12
	26	2.9	54.6	0.07
	27	3.00	50.8	0.09
	28	2.68	51.2	0.08
	29	3.99	57.4	0.07
	30	3.08	53.0	0.09
N=3	1	3.29	50.2	0.11
	2	2.89	53.2	0.15
	3	3.27	49.6	0.08
	4	2.60	50.0	0.11
	5	3.30	49.6	0.07
	6	2.62	59.0	0.06
	7	3.17	51.6	0.12
	8	3.07	52.4	0.11
	9	3.48	49.8	0.07
	10	2.94	51.8	0.14
	11	3.35	51.0	0.07
	12	3.62	50.4	0.09
	13	3.46	51.2	0.08
	14	3.01	53.6	0.09
	15	3.44	52.6	0.20
	16	4.65	54.8	0.09
	17	2.83	46.0	0.11

	18	3.81	55.6	0.09
	19	3.51	53.4	0.07
	20	3.18	50.2	0.14
	21	3.31	50.0	0.09
	22	3.70	59.4	0.14
	23	3.24	50.4	0.06
	24	3.26	54.8	0.13
	25	3.75	49.4	0.07
	26	4.09	56.0	0.12
	27	3.18	47.4	0.10
	28	2.68	54.4	0.11
	29	2.90	50.8	0.01
	30	3.55	57.0	0.04

Table S3. Summary of inter-planar spacing determined from SAED patterns of NT-3DFG.

C-C neighbor	Experimental values (nm)
1 st nearest neighbor	0.123 ± 0.002
2 nd nearest neighbor	0.212 ± 0.005
Inter-layer spacing	0.360 ± 0.002

Table S4. Data summary for XPS analysis (atomic percent) for NT-3DFG before and after surface modifications.

	% Carbon	% Oxygen	% Nitrogen
Pristine	98.8 ± 0.2	1.2 ± 0.2	-
Nitric treated	96.6 ± 0.1	3.4 ± 0.1	trace
Nitric-treated and KF modified	93.9 ± 0.4	4.0 ± 0.2	2.0 ± 0.2

Table S5. Data summary for XPS analysis (peak positions and peak area ratios) for NT-3DFG before and after surface modifications

		pristine		Nitric treated		Nitric and KF modified	
		Peak position (eV)	Peak area ratio	Peak position (eV)	Peak area ratio	Peak position (eV)	Peak area ratio
C1s	C sp²	284.4	1	284.3	1	284.4	1
	C-O	-	-	285.7	0.02	285.7	0.03
	C=O	-	-	286.8	0.03	286.8	0.02
	O=C-O	-	-	288.1	0.03	288.1	0.03
	Shake-up	290.3	0.1	290.4	0.07	290.4	0.04
O1s	C=O	531.9	1	531.8	1	531.9	1
	C-O	533.5	0.9	533.4	0.9	533.2	0.43
N1s	C-NH₂	-	-	-	-	400.2	1
	NO₃⁻	-	-	405.8	1	406.2	0.21

Table S6. Data summary for temperature change as a function of power of the incident laser (635 nm laser, 20 μm spot size, 1 ms pulse width) for isolated NT-3DFG. Results are presented as mean \pm SD (n = 10 measurements per wire).

Power (mW)	NT-3DFG								
	1	2	3	4	5	6	7	8	9
2	1.45 \pm 0.07	1.96 \pm 0.03	2.82 \pm 0.03	1.38 \pm 0.04	1.40 \pm 0.04	1.27 \pm 0.02	1.05 \pm 0.02	1.86 \pm 0.03	1.08 \pm 0.02
4	2.22 \pm 0.09	3.70 \pm 0.05	4.57 \pm 0.09	2.36 \pm 0.03	2.23 \pm 0.04	2.33 \pm 0.02	1.95 \pm 0.02	3.60 \pm 0.04	2.00 \pm 0.02
6	3.56 \pm 0.06	5.76 \pm 0.05	5.98 \pm 0.04	3.24 \pm 0.02	3.04 \pm 0.03	3.33 \pm 0.02	2.66 \pm 0.02	5.09 \pm 0.10	2.87 \pm 0.01
8	4.17 \pm 0.14	7.79 \pm 0.06	6.64 \pm 0.15	3.77 \pm 0.03	3.89 \pm 0.06	4.10 \pm 0.03	3.06 \pm 0.03	6.19 \pm 0.07	3.71 \pm 0.02
10	5.79 \pm 0.19	10.52 \pm 0.08	8.19 \pm 0.50	4.23 \pm 0.02	4.73 \pm 0.05	4.76 \pm 0.03	4.15 \pm 0.02	6.74 \pm 0.07	4.63 \pm 0.03

Table S7. Data summary for temperature change as a function of power of the incident laser (635 nm laser, 20 μm spot size, 10 ms pulse width) for isolated NT-3DFG. Results are presented as mean \pm SD (n = 10 measurements per wire).

Power (mW)	NT-3DFG								
	1	2	3	4	5	6	7	8	9
2	1.75 \pm 0.07	2.40 \pm 0.04	3.77 \pm 0.03	1.72 \pm 0.02	1.93 \pm 0.06	2.00 \pm 0.02	1.83 \pm 0.01	2.40 \pm 0.03	1.57 \pm 0.02
4	2.57 \pm 0.12	4.55 \pm 0.04	6.26 \pm 0.08	3.02 \pm 0.02	3.09 \pm 0.07	3.70 \pm 0.02	3.41 \pm 0.02	4.69 \pm 0.03	2.90 \pm 0.02
6	3.81 \pm 0.14	6.80 \pm 0.05	7.50 \pm 0.88	4.06 \pm 0.02	4.34 \pm 0.06	5.30 \pm 0.02	4.57 \pm 0.04	6.64 \pm 0.05	4.08 \pm 0.01
8	5.11 \pm 0.15	10.00 \pm 0.06	8.98 \pm 0.25	4.88 \pm 0.03	5.56 \pm 0.05	6.60 \pm 0.04	5.18 \pm 0.03	8.10 \pm 0.07	5.31 \pm 0.02
10	7.48 \pm 0.19	12.64 \pm 0.11	9.18 \pm 0.17	5.47 \pm 0.06	6.71 \pm 0.07	7.66 \pm 0.04	7.58 \pm 0.04	8.89 \pm 0.07	6.77 \pm 0.03

Table S8. Data summary for temperature change as a function of power of the incident laser (405 nm laser, 20 μm spot size, 10 ms pulse width) for isolated NT-3DFG. Results are presented as mean \pm SD (n = 10 measurements per wire).

Power (mW)	NT-3DFG								
	1	2	3	4	5	6	7	8	9
2	1.74 \pm 0.04	3.01 \pm 0.01	2.63 \pm 0.05	1.53 \pm 0.05	1.90 \pm 0.03	2.08 \pm 0.04	3.10 \pm 0.05	3.41 \pm 0.04	2.23 \pm 0.06
4	3.52 \pm 0.05	5.25 \pm 0.02	4.58 \pm 0.03	2.68 \pm 0.04	3.29 \pm 0.04	3.67 \pm 0.03	6.16 \pm 0.04	6.20 \pm 0.03	4.26 \pm 0.04
6	4.90 \pm 0.05	7.31 \pm 0.01	6.15 \pm 0.03	3.81 \pm 0.02	4.99 \pm 0.02	5.54 \pm 0.03	8.50 \pm 0.03	9.08 \pm 0.04	6.03 \pm 0.06
8	6.26 \pm 0.04	9.23 \pm 0.02	7.70 \pm 0.03	4.95 \pm 0.02	6.39 \pm 0.04	8.02 \pm 0.04	10.55 \pm 0.02	10.54 \pm 0.04	7.69 \pm 0.04
10	7.96 \pm 0.05	11.13 \pm 0.30	9.04 \pm 0.02	6.12 \pm 0.02	7.30 \pm 0.02	9.94 \pm 0.04	12.69 \pm 0.04	12.14 \pm 0.04	9.39 \pm 0.05

Table S9. Data summary for temperature change as a function of power of the incident laser (635 nm laser, 20 μm spot size, 1 ms pulse width) for isolated bare i-SiNW. Results are presented as mean \pm SD (n = 10 measurements per wire).

Power (mW)	i-SiNW									
	1	2	3	4	5	6	7	8	9	10
2	0.02 \pm 0.01	0.03 \pm 0.01	0.04 \pm 0.01	0.03 \pm 0.01	0.03 \pm 0.01	0.04 \pm 0.01	0.04 \pm 0.01	0.04 \pm 0.01	0.04 \pm 0.02	0.04 \pm 0.01
4	0.03 \pm 0.01	0.07 \pm 0.01	0.04 \pm 0.01	0.03 \pm 0.01	0.03 \pm 0.01	0.04 \pm 0.01	0.04 \pm 0.01	0.04 \pm 0.01	0.04 \pm 0.01	0.04 \pm 0.01
6	0.04 \pm 0.01	0.08 \pm 0.01	0.04 \pm 0.02	0.04 \pm 0.01	0.04 \pm 0.01	0.05 \pm 0.01	0.04 \pm 0.01	0.04 \pm 0.01	0.04 \pm 0.01	0.04 \pm 0.01
8	0.05 \pm 0.01	0.10 \pm 0.02	0.06 \pm 0.01	0.06 \pm 0.01	0.04 \pm 0.01	0.04 \pm 0.01	0.06 \pm 0.01	0.04 \pm 0.01	0.04 \pm 0.01	0.04 \pm 0.01
10	0.06 \pm 0.02	0.12 \pm 0.02	0.04 \pm 0.01	0.06 \pm 0.01	0.04 \pm 0.01	0.05 \pm 0.01	0.06 \pm 0.01	0.04 \pm 0.01	0.04 \pm 0.01	0.04 \pm 0.01
12	0.07 \pm 0.01	0.12 \pm 0.02	0.08 \pm 0.01	0.07 \pm 0.01	0.04 \pm 0.01	0.06 \pm 0.01	0.05 \pm 0.01	0.05 \pm 0.01	0.06 \pm 0.01	0.04 \pm 0.01
14	0.09 \pm 0.01	0.16 \pm 0.02	0.08 \pm 0.01	0.09 \pm 0.02	0.05 \pm 0.01	0.08 \pm 0.02	0.07 \pm 0.02	0.08 \pm 0.01	0.04 \pm 0.01	0.04 \pm 0.01
16	0.09 \pm 0.02	0.20 \pm 0.03	0.09 \pm 0.01	0.07 \pm 0.01	0.05 \pm 0.01	0.08 \pm 0.01	0.08 \pm 0.01	0.08 \pm 0.02	0.04 \pm 0.01	0.06 \pm 0.01
18	0.09 \pm 0.01	0.20 \pm 0.03	0.10 \pm 0.02	0.11 \pm 0.02	0.05 \pm 0.01	0.10 \pm 0.02	0.08 \pm 0.01	0.09 \pm 0.01	0.07 \pm 0.01	0.07 \pm 0.00
20	0.12 \pm 0.02	0.22 \pm 0.03	0.08 \pm 0.01	0.11 \pm 0.03	0.04 \pm 0.01	0.10 \pm 0.02	0.11 \pm 0.02	0.10 \pm 0.02	0.05 \pm 0.01	0.07 \pm 0.01
22	0.14 \pm 0.02	0.26 \pm 0.02	0.09 \pm 0.01	0.11 \pm 0.03	0.05 \pm 0.01	0.12 \pm 0.03	0.10 \pm 0.03	0.12 \pm 0.02	0.07 \pm 0.01	0.05 \pm 0.01

Table S10. Data summary for temperature change as a function of power of the incident laser (635 nm laser, 20 μm spot size, 10 ms pulse width) for isolated bare i-SiNW. Results are presented as mean \pm SD (n = 10 measurements per wire).

Power (mW)	i-SiNW									
	1	2	3	4	5	6	7	8	9	10
2	0.05 \pm 0.01	0.06 \pm 0.02	0.04 \pm 0.01	0.04 \pm 0.01	0.03 \pm 0.01	0.05 \pm 0.01	0.03 \pm 0.02	0.04 \pm 0.01	0.04 \pm 0.01	0.04 \pm 0.01
4	0.07 \pm 0.01	0.11 \pm 0.02	0.07 \pm 0.02	0.06 \pm 0.02	0.05 \pm 0.01	0.07 \pm 0.02	0.06 \pm 0.02	0.07 \pm 0.01	0.06 \pm 0.01	0.06 \pm 0.01
6	0.10 \pm 0.01	0.14 \pm 0.02	0.10 \pm 0.02	0.09 \pm 0.02	0.06 \pm 0.01	0.10 \pm 0.02	0.09 \pm 0.02	0.09 \pm 0.02	0.07 \pm 0.01	0.09 \pm 0.02
8	0.13 \pm 0.01	0.19 \pm 0.03	0.12 \pm 0.02	0.12 \pm 0.03	0.09 \pm 0.02	0.13 \pm 0.02	0.11 \pm 0.02	0.13 \pm 0.02	0.09 \pm 0.02	0.09 \pm 0.01
10	0.16 \pm 0.01	0.23 \pm 0.02	0.14 \pm 0.02	0.15 \pm 0.02	0.11 \pm 0.02	0.15 \pm 0.03	0.14 \pm 0.02	0.14 \pm 0.02	0.12 \pm 0.02	0.12 \pm 0.03
12	0.19 \pm 0.01	0.26 \pm 0.03	0.17 \pm 0.03	0.17 \pm 0.02	0.12 \pm 0.02	0.17 \pm 0.02	0.16 \pm 0.03	0.18 \pm 0.02	0.14 \pm 0.02	0.13 \pm 0.02
14	0.22 \pm 0.02	0.31 \pm 0.02	0.19 \pm 0.02	0.19 \pm 0.02	0.14 \pm 0.02	0.20 \pm 0.03	0.19 \pm 0.03	0.20 \pm 0.02	0.15 \pm 0.02	0.15 \pm 0.03
16	0.24 \pm 0.03	0.35 \pm 0.03	0.22 \pm 0.03	0.23 \pm 0.03	0.16 \pm 0.03	0.23 \pm 0.02	0.22 \pm 0.02	0.22 \pm 0.03	0.18 \pm 0.02	0.17 \pm 0.02
18	0.28 \pm 0.03	0.39 \pm 0.03	0.23 \pm 0.02	0.24 \pm 0.02	0.17 \pm 0.02	0.27 \pm 0.03	0.24 \pm 0.03	0.24 \pm 0.02	0.19 \pm 0.02	0.20 \pm 0.02
20	0.29 \pm 0.02	0.44 \pm 0.03	0.26 \pm 0.02	0.27 \pm 0.03	0.19 \pm 0.03	0.30 \pm 0.02	0.28 \pm 0.03	0.28 \pm 0.02	0.20 \pm 0.03	0.21 \pm 0.02
22	0.32 \pm 0.02	0.49 \pm 0.03	0.28 \pm 0.03	0.29 \pm 0.02	0.21 \pm 0.03	0.31 \pm 0.03	0.30 \pm 0.02	0.29 \pm 0.03	0.22 \pm 0.03	0.21 \pm 0.02

Table S11. Data summary for NT-3DFG suspension concentration quantification.

Sample	Area (mm ²)	NT-3DFG mass/area (µg/mm ²)	NT-3DFG mass (µg)	NT-3DFG concentration in 500 µL 1X PBS (µg/mL)
1	23.75	0.640 ± 0.025	15.15 ± 0.55	30.30 ± 1.10
2	24.00		15.30 ± 0.55	30.60 ± 1.10
3	25.25		16.10 ± 0.60	32.20 ± 1.20
4	22.80		14.55 ± 0.50	29.10 ± 1.00
5	18.85		12.05 ± 0.40	24.10 ± 0.80
6	23.65		15.10 ± 0.55	30.20 ± 1.10

Table S12. Data summary for NT-3DFG concentration quantification.

Concentration	NT-3DFG suspension concentration ($\mu\text{g/mL}$)	NT-3DFG suspension volume (μL)	PBS volume (μL)	NT-3DFG mass (μg)	NT-3DFG concentration ($\mu\text{g/mL}$)
Control	-	-	50	-	-
Concentration 1	29.10 \pm 1.00	10	40	0.30 \pm 0.02	0.15 \pm 0.01
Concentration 2		50	0	1.45 \pm 0.10	0.75 \pm 0.05

Table S13. Data summary for the photothermal stimulation parameters sorted by increasing energy per pulse per neuron (n = 12 DRG neurons).

DRG neuron	Pulse power (mW)	Pulse duration (μs)	Energy per pulse (nJ)
1	13.60	2	27.2
	4.61	8	36.9
	5.74	11	63.2
	4.17	20	83.3
	3.65	60	218.8
	3.02	150	453.0
	2.28	600	1368.0
	2.38	2600	6180.0
2	5.38	60	322.7
	5.32	250	1330.0
	4.42	500	2210.0
	2.28	2400	5472.0
	3.02	2400	7248.0
3	9.69	6	58.1
	6.27	20	125.4
	5.38	65	349.6
	5.32	120	638.4
	4.42	150	663.0
	3.02	700	2114.0
	2.28	1600	3648.0
	2.06	5000	10300.0
4	4.42	200	884.0
	3.02	700	2114.0
	2.28	1300	2964.0
	2.06	2800	5768.0
	1.73	4200	7266.0
5	3.02	500	1510.0
	2.28	800	1824.0
	2.06	1000	2060.0
6	3.02	1800	5436.0
7	2.28	600	1368.0
8	2.28	5000	11400.0
9	3.02	700	2114.0
10	3.02	800	2416.0
11	4.42	200	884.0
	3.02	600	1812.0
12	4.42	800	3536.0

References

1. Garg R, *et al.* (2017) Nanowire-mesh-templated growth of out-of-plane three-dimensional fuzzy graphene. *ACS Nano* 11(6):6301-6311.
2. Garg R, *et al.* (2019) Electron transport in multi-dimensional fuzzy graphene nanostructures. *Nano Letters*.
3. Rastogi SK, *et al.* (2020) Three-dimensional fuzzy graphene ultra-microelectrodes for sub cellular recordings. *Nano Research* doi.org/10.1007/s12274-020-2695-y.
4. Ferrari AC & Basko DM (2013) Raman spectroscopy as a versatile tool for studying the properties of graphene. *Nature Nanotechnology* 8(4):235.
5. Hiramatsu M & Hori M (2010) *Carbon nanowalls: synthesis and emerging applications* (Springer Science & Business Media).
6. Torrisi F, *et al.* (2012) Inkjet-printed graphene electronics. *ACS Nano* 6(4):2992-3006.
7. Döbbelin M, *et al.* (2016) Light-enhanced liquid-phase exfoliation and current photoswitching in graphene–azobenzene composites. *Nature Communications* 7:11090.
8. Ferrari A & Robertson J (2001) Resonant Raman spectroscopy of disordered, amorphous, and diamondlike carbon. *Physical Review B* 64(7):075414.
9. Mattevi C, *et al.* (2009) Evolution of electrical, chemical, and structural properties of transparent and conducting chemically derived graphene thin films. *Advanced Functional Materials* 19(16):2577-2583.
10. Deokar G, *et al.* (2015) Towards high quality CVD graphene growth and transfer. *Carbon* 89:82-92.
11. San Roman D, *et al.* (2020) Engineering Three-Dimensional (3D) Out-of-Plane Graphene Edge Sites for Highly Selective Two-Electron Oxygen Reduction Electrocatalysis. *ACS Catalysis* 10(3):1993-2008.
12. Polzonetti G, *et al.* (2006) Thin films of a self-assembling peptide on TiO₂ and Au studied by NEXAFS, XPS and IR spectroscopies. *Materials Science and Engineering: C* 26(5-7):929-934.
13. Sai L, *et al.* (2017) Protein-derived carbon nanodots with an ethylenediamine-modulated structure as sensitive fluorescent probes for Cu²⁺ detection. *RSC Advances* 7(27):16608-16615.
14. López GP, Castner DG, & Ratner BD (1991) XPS O 1s binding energies for polymers containing hydroxyl, ether, ketone and ester groups. *Surface and Interface Analysis* 17(5):267-272.
15. Araújo MP, Soares O, Fernandes A, Pereira M, & Freire C (2017) Tuning the surface chemistry of graphene flakes: new strategies for selective oxidation. *RSC Advances* 7(23):14290-14301.
16. Stevens JS, *et al.* (2013) Quantitative analysis of complex amino acids and RGD peptides by X-ray photoelectron spectroscopy (XPS). *Surface and Interface Analysis* 45(8):1238-1246.
17. Barazzouk S & Daneault C (2012) Amino acid and peptide immobilization on oxidized nanocellulose: spectroscopic characterization. *Nanomaterials* 2(2):187-205.
18. Landoulsi J, *et al.* (2016) Organic adlayer on inorganic materials: XPS analysis selectivity to cope with adventitious contamination. *Applied Surface Science* 383:71-83.
19. Kasry A, Kuroda MA, Martyna GJ, Tulevski GS, & Bol AA (2010) Chemical doping of large-area stacked graphene films for use as transparent, conducting electrodes. *ACS Nano* 4(7):3839-3844.
20. Fillaux F, *et al.* (1999) Inelastic neutron scattering study of the proton dynamics in HNO₃ graphite intercalation compounds. *Chemical Physics* 242(2):273-281.